Title	Saturated-excitation image scanning microscopy
Author(s)	Temma, Kenta; Oketani, Ryosuke; Lachmann, René et al.
Citation	Optics Express. 2022, 30(8), p. 13825-13838
Version Type	VoR
URL	https://hdl.handle.net/11094/103331
rights	© 2022 Optica Publishing Group. Users may use, reuse, and build upon the article, or use the article for text or data mining, so long as such uses are for non-commercial purposes and appropriate attribution is maintained. All other rights are reserved.
Note	

Saturated-excitation image scanning microscopy

Kenta Temma,[1,2] **Ryosuke Oketani,**[1] **René Lachmann,**[3,4]
Toshiki Kubo,[1] **Nicholas I. Smith,**[5,6] **Rainer Heintzmann,**[3]
and Katsumasa Fujita[1,2,6,*]

[1]*Department of Applied Physics, Osaka University, Suita, Osaka 565-0871, Japan*

[2]*Advanced Photonics and Biosensing Open Innovation Laboratory, AIST-Osaka University, Suita, Osaka 565-0871, Japan*

[3]*Institute of Physical Chemistry and Abbe Center of Photonics, Friedrich-Schiller-University Jena, Helmholtzweg 4, 07743 Jena, Germany*

[4]*Leibniz Institute of Photonic Technology, Albert-Einstein Str. 9, 07745 Jena, Germany*

[5]*Immunology Frontier Research Center, Osaka University, Suita, Osaka 565-0871, Japan*

[6]*Institute for Open and Transdisciplinary Research Initiatives, Osaka University, Suita, Osaka 565-0871, Japan*

[*]*fujita@ap.eng.osaka-u.ac.jp*

Abstract: Image scanning microscopy (ISM) overcomes the trade-off between spatial resolution and signal volume in confocal microscopy by rearranging the signal distribution on a two-dimensional detector array to achieve a spatial resolution close to the theoretical limit achievable by infinitesimal pinhole detection without sacrificing the detected signal intensity. In this paper, we improved the spatial resolution of ISM in three dimensions by exploiting saturated excitation (SAX) of fluorescence. We theoretically investigated the imaging properties of ISM, when the fluorescence signals are nonlinearly induced by SAX, and show combined SAX-ISM fluorescence imaging to demonstrate the improvement of the spatial resolution in three dimensions. In addition, we confirmed that the SNR of SAX-ISM imaging of fluorescent beads and biological samples, which is one of the challenges in conventional SAX microscopy, was improved.

1. Introduction

Confocal laser scanning microscopy enables fluorescence imaging with a spatial resolution beyond the classical diffraction limit by employing the detection pinhole with a diameter smaller than the Airy disk (one Airy unit, AU) [1,2]. However, in practice, the trade-off between the spatial resolution and detectable signal hinders super-resolution confocal microscopy. Image scanning microscopy (ISM) overcomes this trade-off by utilizing a detector array to detect the spatial distribution of the signal excited by the laser focus [3,4]. Digital or optical rearrangement of the signal distribution can then compensate for the displaced signal distribution on the detector array in order to retrieve the high-spatial frequency components transferred through the confocal setup [4–8]. ISM has been applied for two-photon excitation imaging [9,10], super-resolution optical fluctuation imaging [11], fluorescence lifetime imaging [12], and Raman imaging [13] to improve both spatial resolution and signal-to-noise ratio (SNR) simultaneously.

In this research, we improved the spatial resolution of ISM by introducing saturated excitation (SAX) of fluorescence. SAX microscopy improves the spatial resolution of laser scanning microscopy in three dimensions by exploiting nonlinear fluorescence responses induced by saturation of fluorescence [14]. SAX microscopy is also useful for high-resolution imaging of relatively thick samples, such as 3D cultured cells, because the signal localization within the excitation focus effectively eliminates the out-of-focus background [15]. The resolution improvement obtained by SAX is unlimited in theory, but practically limited by the signal to

noise ratio (SNR) in fluorescence detection, as higher-order nonlinear fluorescence signals are typically weak and hidden by noise. Therefore, the combination of SAX and ISM can improve the practical spatial resolution of SAX microscopy without compromising the signal level of a conventional confocal setup. In this research, we developed a technique to implement the SAX technique to ISM, and investigated the imaging property of SAX-ISM including optimization of the rearrangement of nonlinear signals. We also developed an optical system for SAX-ISM, and experimentally confirmed the improvement of spatial resolution and SNR.

2. Theory

In ISM, a detector array, which consists of multiple light-detection elements, captures the distribution of fluorescence emission excited by a laser focus, and the signal distribution is spatially reassigned to compensate for the displacement of signal distribution due to light detection at off-axis positions. The point-spread function (PSF) of ISM can be provided as the sum of spatially-shifted PSF ($h_{\mathrm{eff}_{ij}}$) given by each detector element as described in previous literature [4,5].

$$h_{\mathrm{ISM}}(r) = \sum_{i,j=0}^{n} h_{\mathrm{eff}_{ij}}(r - a r_{ij}) \tag{1}$$

r is a radial coordinate in the sample plane. r_{ij} is zero when the detector element is on the optical axis. a is the reassignment factor (RF) applied for each effective PSF at summation. The effective PSF obtained by using a detector element at a position r_{ij} is given as,

$$h_{\mathrm{eff}_{ij}}(r) = h_{\mathrm{ex}}(r)\{ h_{\mathrm{det}}(r - r_{ij}) \otimes D\} \tag{2}$$

in Ref. [3], where h_{ex} and h_{det} are the intensity PSFs of the excitation and the detection system, respectively. D is the spatial distribution of the sensitivity of the detector element.

In SAX-ISM, saturated excitation provides an excitation PSF size smaller than that by linear excitation (i.e. typical ISM), and the effective PSF for SAX-ISM can be rewritten as,

$$h_{\mathrm{eff-SAX}_{ij}}(r) = h_{\mathrm{SAX}}(r)\{ hdet(r - r_{ij}) \otimes D\} \tag{3}$$

where h_{SAX} is an excitation PSF in SAX microscopy that can be obtained by the differential saturated excitation (dSAX) technique [16,17]. We assumed that 488 nm light was focused by an NA-1.3 objective lens for excitation. We used a vector calculation to obtain the electric field distribution at the focus assuming circular polarization [18]. The detection PSFs were calculated using a fluorescence emission wavelength of 515 nm and a square-shaped detector with a size of 0.2 AU. To estimate the excitation PSF in SAX microscopy, we calculated saturated and unsaturated excitation PSFs assuming Rhodamine 6G as a fluorescent specimen and took the difference by using the dSAX method. To calculate the saturated excitation PSFs, the relation between excitation and fluorescence intensities of Rhodamine 6G was calculated by solving the rate equation at steady-state conditions for a five-level energy system using the photophysical parameters as described in [19].

Figure 1(a)-(c) show the effective PSFs of linear confocal and SAX microscopy obtained at different single detector elements. We confirmed that the displacement of the effective PSFs in case of displaced detector elements are different for linear confocal and 2$^{\mathrm{nd}}$, 3$^{\mathrm{rd}}$ order SAX microscopy. Therefore, the optimal reassignment shift should be chosen for each excitation mode. As reported for ISM using multiphoton and Bessel beam excitation [20–22], an optimized RF depends on the shape and widths of excitation and detection PSFs. As indicated in Fig. 1(a)-(c), the RF for SAX-ISM should be different for the order of nonlinearity used for imaging.
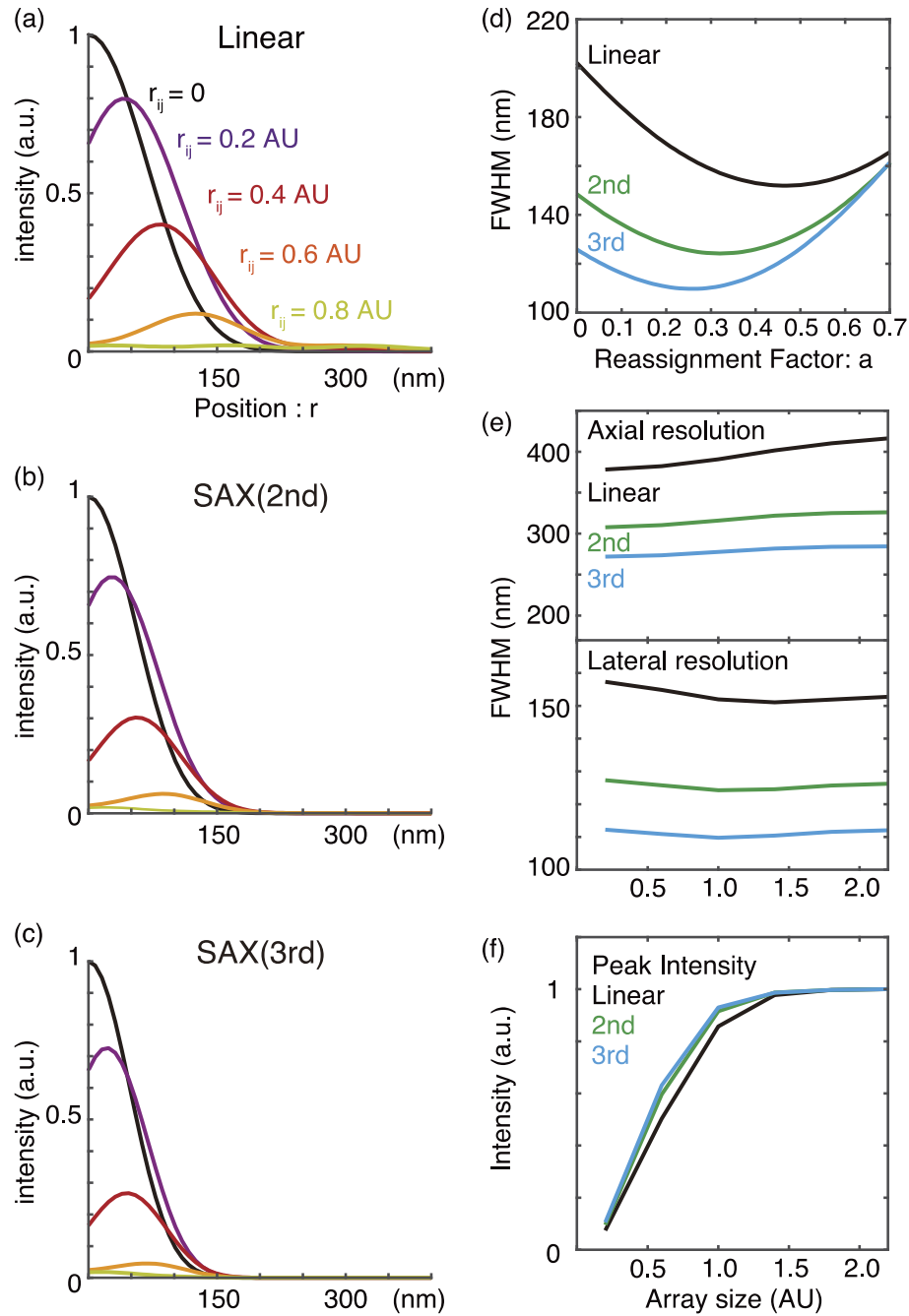
Fig. 1. Cross section through calculated effective PSFs of (a) linear confocal and (b) 2nd, (c) 3rd order SAX microscopy using a single square detector element with a size of 0.2 AU shifted with distances of between 0 to 0.8 AU from the optical axis. Excitation and emission wavelengths are 488 nm and 515 nm, respectively. A silicone-immersion objective lens (refractive index: 1.406) with an NA of 1.3 was assumed. (d) Relationship between the reassignment factor (RF) and the lateral FWHM of effective PSF in linear ISM and SAX-ISM. (e) The FWHMs and (f) the peak intensity of effective PSF of SAX-ISM with different array sizes calculated with RFs of 0.47, 0.32, and 0.26 for ISM, 2nd -, and 3rd -order SAX-ISM, respectively. The peak intensity was normalized by the maximum intensity of each excitation mode.

We calculated the effective PSFs obtained using linear, 2nd-order nonlinear, and 3rd-order nonlinear fluorescence responses with different RFs using the following equation.

$$h_{\text{SAX-ISM}}(r) = \sum\nolimits_{i,j=0}^{n} h_{\text{eff-SAX}_{ij}}(r - ar_{ij}) \tag{4}$$

where the effective PSFs provided by the different detector elements are summed with different displacement values (ar_{ij}). Figure 1(d) shows the relationships between RFs and the lateral spatial resolution (FWHM) obtained using linear and 2nd, 3rd order nonlinear response. From these calculations, we found that the RFs of 0.47, 0.32, and 0.26 achieve the highest resolution in linear ISM, 2nd -, and 3rd -order SAX-ISM, respectively.

We also calculated the spatial resolution and the detectable signal amount with different array sizes which consist of different numbers of 0.2 AU square detector elements, as shown in Fig. 1(e) and 1(f), respectively. Detector elements are arranged in a square grid with a 0.2 AU separation so as not to overlap. The calculation conditions were identical to the previous calculations shown in Fig. 1(a)–1(c). We used the optimum RFs for achieving the highest lateral spatial resolution obtained by the calculation in Fig. 1(d). The calculation results show that the axial resolution (FWHM) is degraded as the size of the array increases. On the other hand, the lateral resolution is high at around 1.4, 1.0, 1.0 AU for linear ISM, 2nd- and 3rd-order SAX-ISM.

Figure 1(e) also shows that, with the AUs above those values, the deformation of PSFs, which is seen in Fig. 1(a), $r_{ij} = 0.8$ AU, degraded the spatial resolution. Figure 1(f) shows that the detectable signal increases with a larger array and is closed to the maximum value when the array size was 1.0 AU. We chose a detector array with a size of 1.0 AU for our experiment based on these calculation results, which provide a reasonably high signal without sacrificing the spatial resolution.

We calculated the optical transfer functions (OTFs) of linear ISM, 2nd, 3rd order SAX-ISM and 3rd order conventional SAX microscopy to compare their spatial frequency responses. The OTFs were obtained by the 3D Fourier transform of the effective PSFs. The OTFs were normalized by the peak value and plotted in logarithmic scale within the signal range of 3 dB in Fig. 2. The OTFs show that SAX-ISM support higher spatial frequency in both lateral and axial direction compared to the linear ISM, because the localization of fluorescence signal occurs due to the nonlinear relationship between excitation and emission. In comparison between 3rd order SAX-ISM and conventional SAX microscopy, SAX-ISM supports higher lateral frequency owing to the reassignment process. The axial frequency is comparable with the 0.2 AU confocal detection of conventional SAX microscopy. SAX-ISM provides both lateral and axial resolution similar to conventional SAX microscopy with a small pinhole even when using a larger detector array for capturing higher amounts of signal. The cut-off frequency in SAX-ISM can be increased by a factor of $n+1$ with n being the order nonlinear response compared to wide-field imaging. However, due to the limitation of the signal, it is difficult to reach this cut-off under practical conditions.
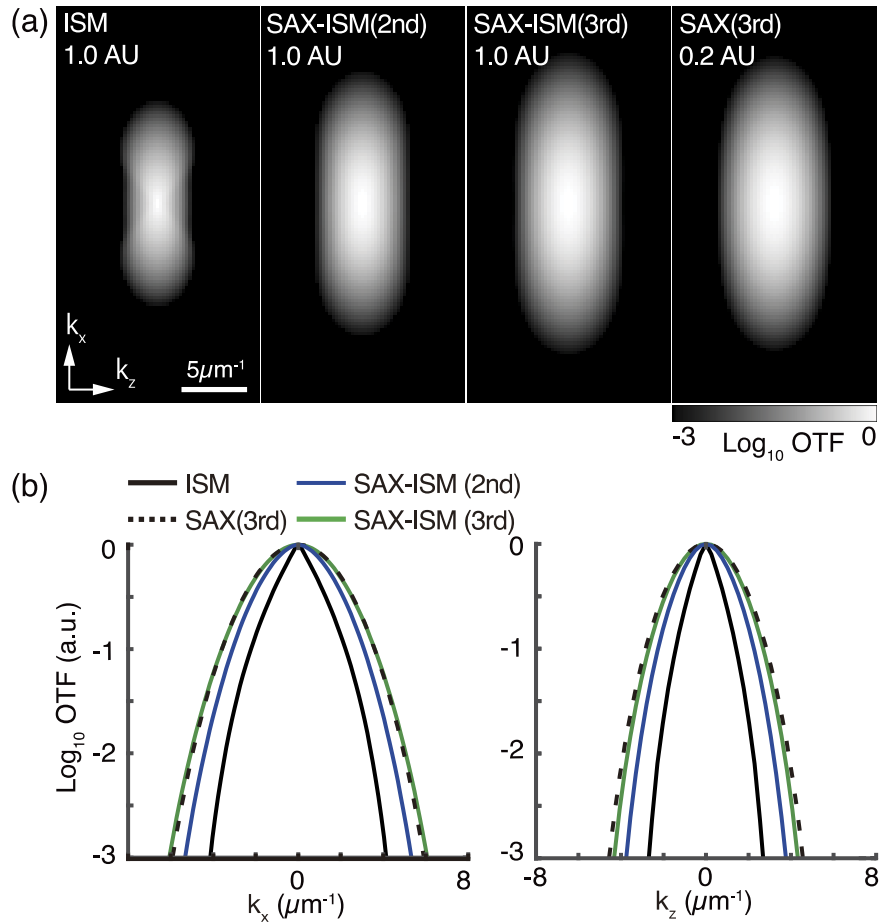
Fig. 2. (a) Optical transfer functions (OTFs) of linear ISM, 2nd, 3rd order SAX-ISM, with a square detector-array with a side length of 1.0 AU and conventional SAX microscopy with a pinhole of diameter 0.2 AU. Each OTF was normalized to its individual maximum and plotted on a logarithmic scale. (b) Line profiles of OTFs in k_x and k_z direction at $k_z = 0$ and $k_z = 0$, respectively. Each profile is normalized by the peak intensity and plotted on a logarithmic scale.

3. Optical setup of SAX-ISM

We built an optical setup of SAX-ISM shown in Fig. 3. A continuous-wave laser with a wavelength of 488 nm (Sapphire 488, Coherent, Inc.) was used as an excitation light source. An acousto-optic modulator (AOM-405AF1, IntraAction) was used for applying a temporal modulation in the excitation intensity. A pair of two lenses and a pinhole were used to expand the excitation beam and fill the objective pupil with the laser beam. The excitation beam was focused onto the sample by using a silicone-immersion objective lens (UPlanSApo 60×/1.30 Sil, Olympus Corporation). The focal spot was scanned by two galvanometer mirrors (6210HBR, Cambridge Technology) in the lateral (x and y) directions. A single-axis piezo stage (P-541, ZCL, PI) was used for scanning the sample in the axial (z) direction. Fluorescence from the excitation spot was collected by the same objective lens and separated from the excitation light by using a short-pass dichromatic reflector (FF505-SDi01-25×36, Semrock) and a long-pass (LP02-488RU-25, Semrock) filter. A lens pair was used to adjust the magnification at the detection plane so as to set the equivalent size of the detector pixel to 0.2 AU. A pinhole with a diameter of 2.0 AU was placed at an intermediate image plane to remove the fluorescence signal from positions far from the focal plane. The fluorescence was imaged on an EMCCD camera (ProEM1024-B, Princeton Instruments) to obtain the intensity distribution of the fluorescence spot, where 5×5 detection pixels form a square detector-array with a side length of 1.0 AU. We employed the intensity modulation within a single pixel in imaging and obtained saturated and unsaturated images with a single scan to avoid artifact generation at the image processing stage. The modulation of excitation light and the camera exposure were synchronized with laser scanning by using a trigger from a function generator (AFG3102C, Tektronics). Detailed imaging protocol and analytical step are explained in the Supplement 1.
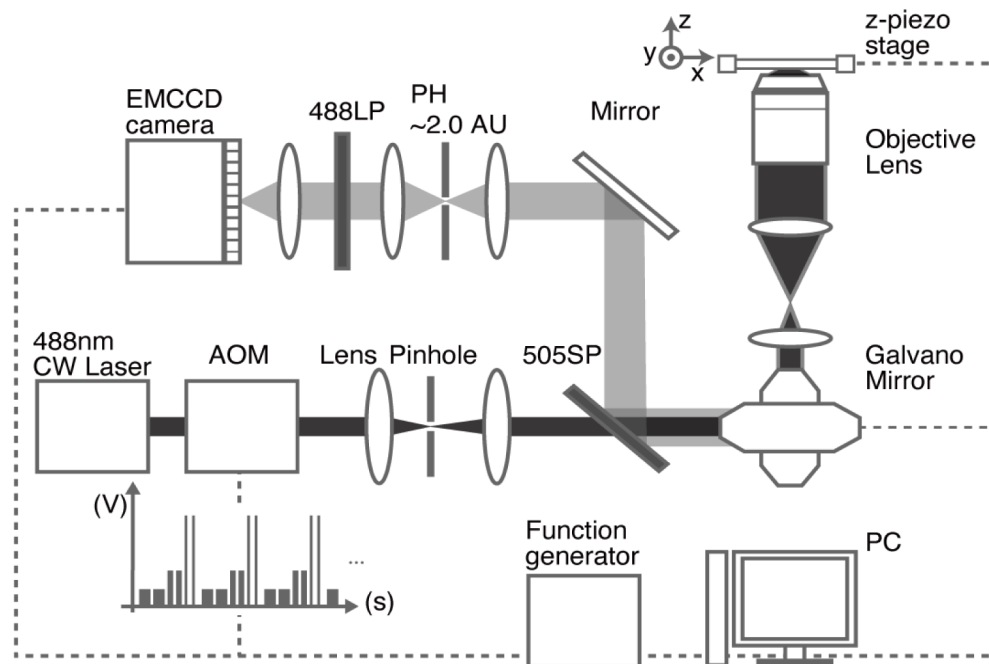

Fig. 3. Optical setup for SAX-ISM (AOM: Acousto-optic modulator, PH: Pinhole, LP: Long Pass Filter, SP: Short Pass Filter)

4. Evaluation of the spatial resolution by ISM in SAX imaging of fluorescence beads

Using the setup above, we observed fluorescent beads (F8803, ThermoFisher scientific) with a diameter of 100 nm to confirm the resolution improvement in SAX-ISM. In brief, we obtain saturated and unsaturated fluorescence images with different excitation intensities and estimated the nonlinear signal components induced by the saturated excitation by an appropriately scaled subtraction. We set the excitation peak irradiance at 91, 263, and 850 (W/cm^2) for obtaining images with three differential excitation irradiances to extract 2nd- and 3rd-order nonlinear SAX-ISM images. The scanning speed was limited to 5 (ms/pixel) due to the framerate of the camera. We reduced the laser irradiation time per pixel to 2 ms by using AOM modulation for all the excitation conditions to reduce photobleaching. Images are reconstructed using Eq. (4) with reassignment factors of 0.47, 0.32, and 0.26 for linear, 2nd- and 3rd-order nonlinear responses obtained by the theoretical calculation in Fig. 1(d), respectively.
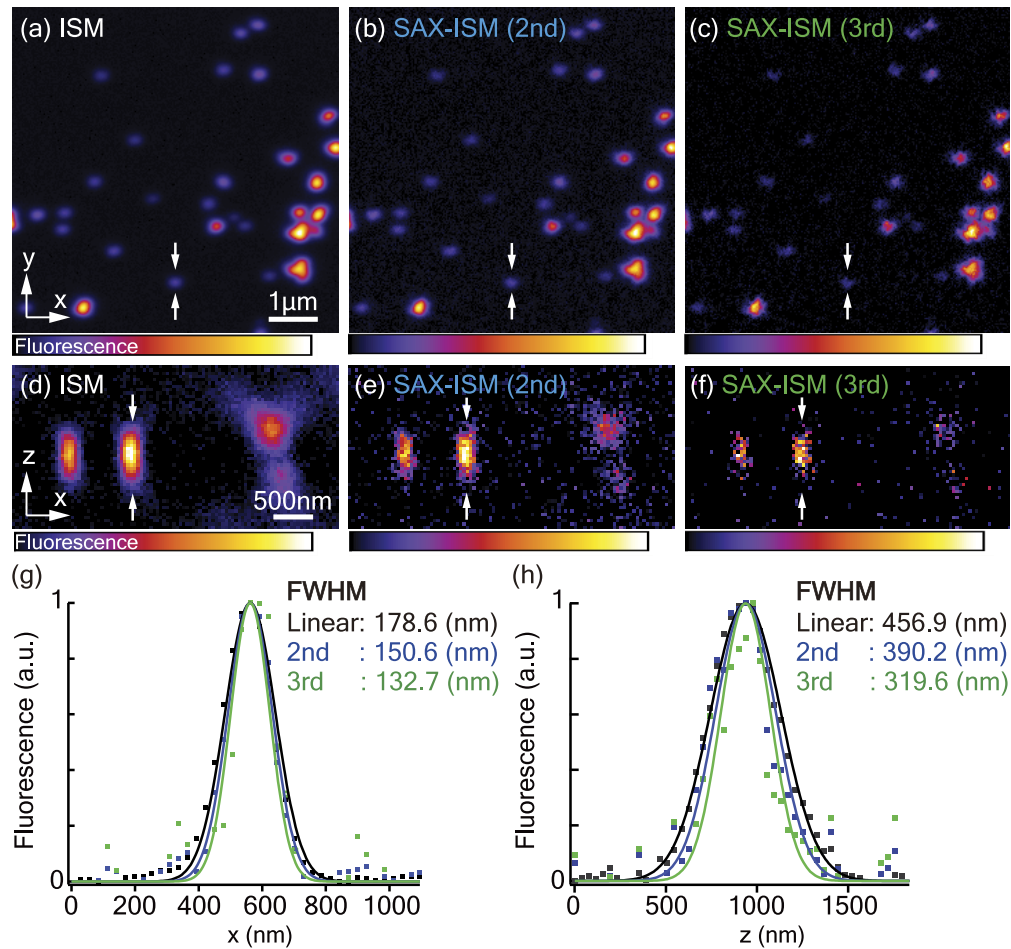

Fig. 4. Measured images of fluorescence beads with 100 nm diameter obtained by linear ISM and SAX-ISM in (a)-(c) x-y and (d)-(f) x-z planes. The intensity profile of a representative bead between white arrowheads and Full Width at Half Maximum (FWHM) calculated via Gaussian fitting in x and z direction are shown in (g), (h).

Figure 4 shows measured fluorescence images of the fluorescence beads in the lateral (x-y) plane reconstructed using (a) linear, (b) 2nd- and (c) 3rd-order nonlinear responses with reassignment along both x and y directions. The intensity profiles and the results of Gaussian fitting of a representative bead indicated by the white arrowheads in (a)-(c) are shown in Fig. 4(g). We also averaged FWHMs of five different fluorescent bead images and obtained 183.1 ± 4.8, 157.1 ± 8.3, and 139.3 ± 10.1 nm for the images using linear, 2nd- and 3rd-order nonlinear responses. These results confirm that extracting the nonlinear fluorescence response improved the spatial resolution in ISM. We also confirmed the resolution improvement in the axial direction by observing x-z images of fluorescent beads under the same excitation condition as the x-y imaging. The fluorescence images and the intensity profiles of fluorescence beads are shown in Fig. 4(d)–4(f) and 4(h). The FWHMs of the z-profile of the bead shown with the white arrows amounted to 456.9, 390.2, and 319.6 nm for linear and 2nd- and 3rd-order SAX-ISM images, respectively, indicating that the use of saturated excitation can extend the spatial resolution in three dimensions in ISM using the lateral reassignment procedure.

## 5.   Comparison of spatial frequency distribution of the image

We compared spatial frequency distributions to evaluate the SNR that could be improved by the addition of image scanning into SAX microscopy, which practically increase the spatial resolution and image contrast in SAX imaging. We used fluorescence images reconstructed from the 3rd-order nonlinear fluorescence response obtained by SAX-ISM and conventional SAX microscopy using differential excitation, as shown in Fig. 5. The 3rd-order conventional SAX image was obtained with above mentioned setup and reconstructed with the same subtraction procedure as SAX-ISM, but the images were reconstructed by integrating the detected signal at the detector array with a size of 0.6 AU (3×3 detector pixels), with which we can compare the signal amount of SAX-ISM and conventional SAX microscopy with a spatial resolution close to the theoretical limit of 3rd order nonlinear mode. The intensity profiles of a representative bead indicated by the white arrowheads in (a) and (b) are shown in Fig. 5(c). The experimental result shows the 2.24 ± 0.16 times signal increase in the peak intensity averaged using five fluorescent bead images by SAX-ISM, which is close to the theoretical evaluation provided in the Supplement 1 (Fig.S1). We applied a 2D Fourier transformation to both images to estimate the noise components that appear in the frequency domain. To compare the contributions of high frequency noise in both images, the spatial frequency distributions were normalized by the value at $0.6\,\mu m^{-1}$, which was the highest value except for the DC component. Figure 5(d) indicates that SAX-ISM has a relatively lower noise contribution at the high spatial frequency region compared to conventional SAX microscopy, which is presumably due to the improvement of the SNR. The relative noise level at 12.0–$13.5\,\mu m^{-1}$ appeared 1.47 times lower in SAX-ISM in Fig. 5(d). This result indicates that the use of SAX-ISM can provide better contrast in imaging high spatial-frequency components, resulting in the improvement of the spatial resolution in practice.
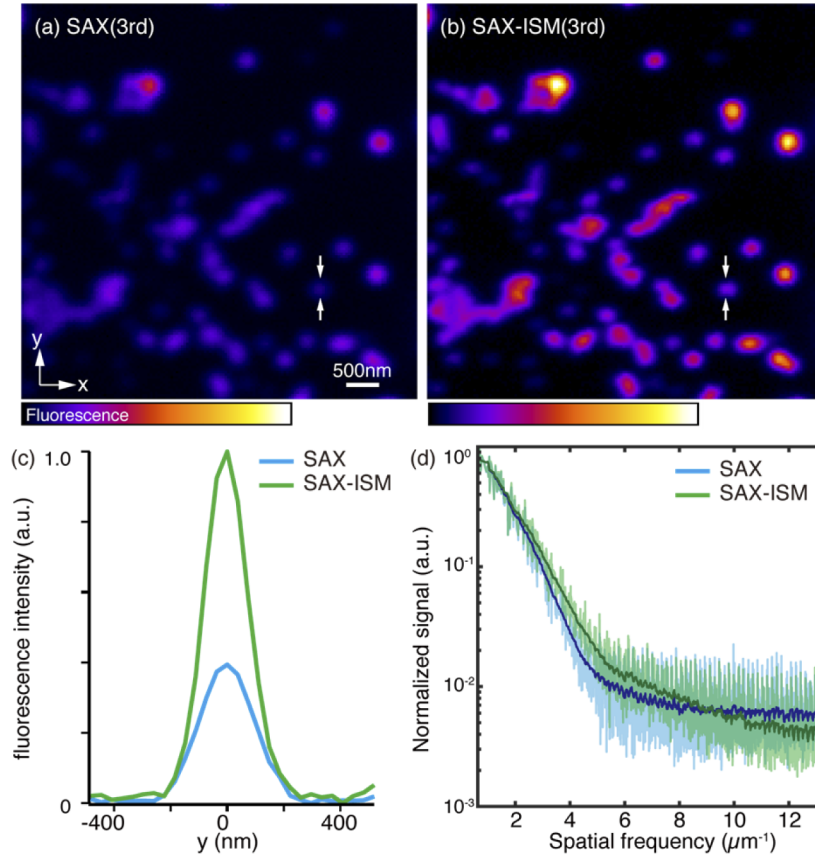
Fig. 5. Measured fluorescence images reconstructed from 3rd order nonlinear response with (a) conventional SAX microscopy by integrating the detected signal at the 0.6 AU size detector array. and (b) SAX-ISM using a detector array size of 1.0 AU with the RF value of 0.26. Peak excitation intensities are 0.3, 0.8 and 2.5 (kW/cm^2) for differential excitation. Excitation light is modulated by rectangular pulses with pulse width and period of 100 µs and 500 µs. The intensity profile of a representative bead between white arrowheads as shown in (c). The signal intensity was normalized by the peak intensity in SAX-ISM to compare the signal amounts. (d) The radial Frequency distribution of each image obtained via 2D Fourier transformation. Fluorescence signals at the same spatial frequency were averaged azimuthally. The dark colored plots are the moving average of 30 radial frequency data points.

6.   Imaging of biological samples

We obtained fluorescence images of HeLa cells to demonstrate the capability of imaging biological specimens. Actin filaments in HeLa cells were stained with Alexa488 phalloidin conjugate (ThermoFischer, A12379). The stained HeLa cells were immersed in an anti-photobleaching agent (ThermoFischer, ProlongGlass Antifade Mountant). We used pulsed excitation to reduce photobleaching. Pulse widths of each excitation intensity were 300 μs, 200 μs, and 100 μs for 1.38, 3.64, and 10.9 (kW/cm^2), respectively. The pulsed excitation was repeated after a 1.3 ms interval, and the pixel dwell time was 5 ms for each excitation intensity. In SAX microscopy using differential excitation, the SNR of extracted nonlinear images is mainly determined by the SNR of a linear image obtained with low excitation intensity, which gives relatively low numbers of fluorescence photons. Therefore, the longer pulse durations were used for lower excitation intensities to achieve a SNR sufficiently high to extract the nonlinear signals as shown in Fig. 3 diagram.
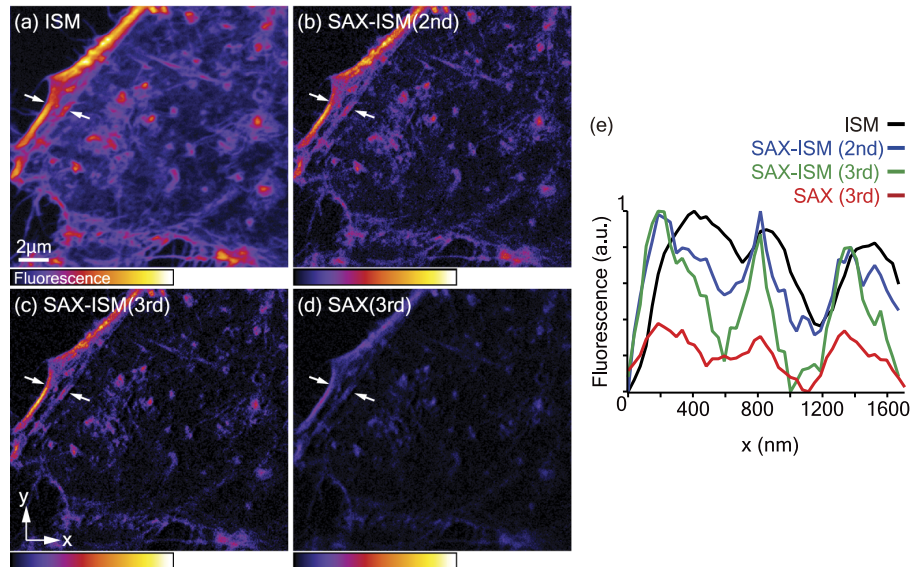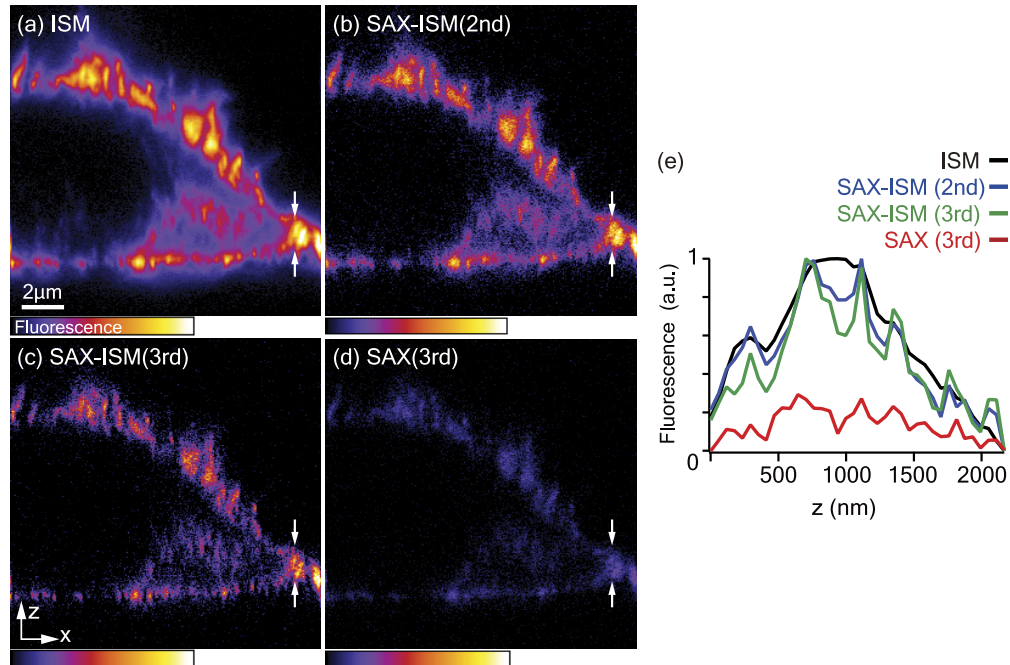

Fig. 6. Measured fluorescence images of actin filaments in a fixed HeLa cell observed by (a) linear ISM, (b) 2nd-, (c) 3rd- order SAX-ISM, and (d) 3rd-order conventional SAX microscopy. The image area and the pixel size are 20×20 μm^2 and 39.1 nm, respectively. The signal intensity in (a)-(c) was normalized by the peak intensity in (a)-(c) to allow a comparison of the spatial resolution between the images. The signal intensity in (d) was normalized by the peak intensity in 3rd -order SAX-ISM so that the signal amounts can be compared between SAX-ISM and conventional SAX microscopy. (e) Intensity profiles of the same position in each image are indicated by the white arrowheads in (a).

In Fig. 6, x-y fluorescence images of the HeLa cells reconstructed using (a) linear ISM, (b) 2nd-, (c) 3rd-order SAX-ISM, and (d) 3rd-order conventional SAX images are shown. The imaging area was 20 μm × 20 μm and the pixel width of the image corresponds to 39.1 nm spacing in the sample plane for x and y directions. The 3rd-order conventional SAX image was obtained by integrating the detected signal with the detector array size of 0.6 AU (3×3 detector pixels) to compare the signal amount with SAX-ISM under the condition that the spatial resolution is close to the theoretical limit. Comparing Fig. 6(a)–6(c), we can confirm the spatial resolution and the image contrast are significantly improved in SAX-ISM compared to conventional linear ISM. Figure 6(e) shows the intensity profile measured at the position indicated by the white

arrowheads in Fig. 6(a), and we can confirm that finer structures are resolved in the images reconstructed by using SAX-ISM. The intensity profile of the conventional SAX image is also shown in Fig. 6(e), where the intensity is normalized by the peak intensity in the line profile of the 3rd-order SAX-ISM image. Comparison of the line profiles of 3rd-order SAX-ISM and conventional SAX shows the increase of the maximum fluorescence signals by a factor of 2.65 by applying the image scanning technique in SAX microscopy.

We also observed an x-z cross-sectional image of a fixed HeLa cell. Excitation conditions were identical to the ones of Fig. 6. The imaging area was $15\,\mu m \times 15\,\mu m$, and the pixel width of the image corresponds to 58.6 nm spacing in the sample plane for x and z directions. Fluorescence images were reconstructed in the same manner as for Fig. 6. Linear ISM, 2nd, 3rd order SAX-ISM, and 3rd order conventional SAX images are shown in Fig. 7(a)–7(d). Figure 7(e) shows the intensity profiles measured at the same position in each image. The position is indicated shown by the white arrowheads in Fig. 7(a). We can confirm the resolution improvement in both x and z directions by SAX-ISM from the comparison of Fig. 7(a), 7(b), and 7(c). The background signal is drastically suppressed by extracting the nonlinear fluorescence response in Fig. 7(b) and 7(c). The comparison of Fig. 7(c) and 7(d) shows that the image scanning technique can extract saturation-induced nonlinear signals more efficiently than the conventional SAX technique.

Fig. 7. Fluorescence images of actin filaments in a fixed HeLa cell observed by (a) linear ISM, (b) 2nd-, (c) 3rd- order SAX-ISM, and (d) 3rd-order conventional SAX microscopy. The image area and the pixel size are $15 \times 15\ \mu m^2$ and 58.6 nm, respectively. The signal intensity in (a)-(c) was normalized by the peak intensity in (a)-(c) to allow a comparison of the spatial resolution between the images. The signal intensity in (d) was normalized by the peak intensity in 3rd -order SAX-ISM so that the signal amounts can be compared between SAX-ISM and conventional SAX microscopy. (e) Intensity profiles of the same position in each image are indicated by the white arrowheads in (a).

7. Conclusions and discussions

In this research, we developed SAX-ISM to improve spatial resolution of ISM in three dimensions. We confirmed that significant improvement in the spatial resolution of ISM can indeed be achieved by the combination with saturated excitation. Both theoretical models and experimental results show that this approach is viable for high spatial resolution and high SNR imaging, with no particular constraints on choice of fluorophore. We estimated the spatial resolution and the signal amount with different RF values in the reassignment process and found that the different RF values give the highest theoretical spatial resolution depending on the nonlinearity of the fluorescence response that determines the size of excitation PSF. We confirmed the resolution improvement by imaging fluorescent beads, extracting saturation-induced nonlinear fluorescence signal in the ISM mode. The nonlinear nature of saturated excitation improved the spatial resolution in all three dimensions using standard lateral reassignment, without additional processing such as weighted averaging [23]. In addition, we experimentally confirmed a 1.47-fold SNR improvement in images of fluorescent beads reconstructed from the 3rd order nonlinear response obtained by SAX-ISM, compared to SAX microscopy realizing theoretically limited resolution (with a 0.6 AU pinhole). The improvement of SNR contributes to extend the detection limit for the high spatial frequency information delivered by nonlinear fluorescence signals in SAX, which improves the practical spatial resolution. We demonstrated the capability can be extended to three-dimensional imaging in a biological sample, without any significant tradeoffs. SAX-ISM provides improvement in the 3D spatial resolution compared to conventional ISM and improves SNR compared to SAX microscopy, so that the combination of the two methods is highly complementary. Implementing SAX into ISM improves the image contrast by eliminating out-of-focus signals in the observation of thick samples.

For further improvement of the spatial resolution, applying deconvolution techniques can be useful for SAX-ISM. Although the practical improvement is limited by the SNR, the expansion of the cut-off frequency by SAX-ISM potentially offers resolution improvement by a factor of $n+1$ with n being the order nonlinear response, compared to the diffraction limit. Even using a nonlinearity of relatively low order, the improvement of SNR by ISM is practically beneficial to increase the effectiveness of deconvolution for the resolution improvement. The higher order of nonlinear signal can be used for further improvement of the spatial resolution when the amount of fluorescence signal is sufficient to extract the weak nonlinear signals. As an example, we have extracted the 4th-order nonlinear response in the imaging of non-bleaching fluorescent nanodiamonds [24]. Photobleaching can be an issue under high excitation intensity used for higher degrees of saturation. However, this can be mitigated in the implementation of SAX-ISM. As discussed in [17], the dSAX technique used in SAX-ISM utilizes pulsed laser light for excitation, which allows us to reduce the average power by tuning the pulse width, while maintaining the degrees of saturation. In our experiment, we did not observe significant photobleaching during the measurement of 3rd order nonlinear signals.

SAX-ISM basically shares the same optical setup with the conventional ISM. However, it is necessary to choose the excitation intensity to obtain high SNR and spatial resolution in SAX images. We measured the saturation curve of fluorescence response to determine the excitation intensities. Since the excitation saturation depends on the chemical environment surrounding fluorescent molecules, the optimal excitation intensities should be estimated under the same condition of imaging measurement. Therefore, we estimated the excitation saturation using the imaging-based technique mentioned in the Supplement 1. In addition, we set the excitation intensity for the unsaturated image as high as possible without photobleaching because the accuracy of the nonlinear signal in the subtraction process also depends on the SNR of the unsaturated fluorescence image. We also chose the excitation intensity for the saturated image to be as small as possible within the range showing excitation saturation to provide better spatial resolutions [25].

SAX-ISM has similarities with scanning based nonlinear structured illumination microscopy (SIM) [26] in terms of using a focal spot for excitation and nonlinearity in fluorescence response induced by saturated excitation. Both imaging properties are quite similar. The difference is that SAX-ISM requires less numbers of fluorescence images to extract super resolution images. For example, the 2nd order nonlinear image reconstruction needs 2 images in SAX and 15 images by scanning SIM. Scanning SIM was also demonstrated using fluorescent nanodiamonds, which are highly resistant to photobleaching, and can produce high SNR images, compared to fluorescent beads or stained biological samples used here. Widefield based nonlinear SIM [27] is also a similar technique. The difference is that SAX-ISM is based on the confocal microscopy, which is useful to visualize the thick specimen. On the other hand, nonlinear SIM can enhance the high frequency information due to the illumination OTF derived from sinusoidal illumination pattern. In our current setup, the temporal resolution is restricted by the framerate of the EMCCD camera. This can be solved by replacing the detector with other sensors such as a photomultiplier-tube array, as used in Airyscan (Zeiss) [28], or an avalanche photodiode array [12]. Multi-spot excitation is also worth exploring as an avenue to increase framerate and/or throughput of this approach for faster imaging [29,30].

Disclosures. The authors declare no conflicts of interest.

Data availability. Data underlying the results presented in this paper are not publicly available at this time but may be obtained from the authors upon reasonable request.

Supplemental document. See Supplement 1 for supporting content.

References

1. T. Wilson and C. J. R. Sheppard, "*Theory and Practice of Scanning Optical Microscopy*," Acad. Press 73 (1984).
2. T. Wilson, "Resolution and optical sectioning in the confocal microscope," J. Microsc. **244**(2), 113–121 (2011).
3. C. J. R. Sheppard, "Superresolution In Confocal Imaging," Optik (Stuttg). **80**, (1988).
4. C. B. Müller and J. Enderlein, "Image scanning microscopy," Phys. Rev. Lett. **104**, 198101 (2010).
5. C. J. R. Sheppard, S. B. Mehta, and R. Heintzmann, "Superresolution by image scanning microscopy using pixel reassignment," Opt. Lett. **38**(15), 2889 (2013).
6. S. Roth, C. J. R. Sheppard, K. Wicker, and R. Heintzmann, "Optical photon reassignment microscopy," Opt Nano **2**(1), 5 (2013).
7. A. G. York, P. Chandris, D. D. Nogare, J. Head, P. Wawrzusin, R. S. Fischer, A. Chitnis, and H. Shroff, "Instant super-resolution imaging in live cells and embryos via analog image processing," Nat. Methods **10**(11), 1122–1126 (2013).
8. I. Gregor, M. Spiecker, R. Petrovsky, J. Großhans, R. Ros, and J. Enderlein, "Rapid nonlinear image scanning microscopy," Nat. Methods **14**(11), 1087–1089 (2017).
9. S. Sun, S. Liu, W. Wang, Z. Zhang, C. Kuang, and X. Liu, "Improving the resolution of two-photon microscopy using pixel reassignment," Appl. Opt. **57**(21), 6181 (2018).
10. S. V. Koho, E. Slenders, G. Tortarolo, M. Castello, M. Buttafava, F. Villa, E. Tcarenkova, M. Ameloot, P. Bianchini, C. J. R. Sheppard, A. Diaspro, A. Tosi, and G. Vicidomini, "Two-photon image scanning microscopy with SPAD array and blind image reconstruction," Biomed. Opt. Express **11**(6), 2905–2924 (2020).
11. A. Sroda, A. Makowski, R. Tenne, U. Rossman, G. Lubin, D. Oron, and R. Lapkiewicz, "SOFISM: Super-resolution optical fluctuation image scanning microscopy," Optica **7**(10), 1308 (2020).
12. M. Castello, G. Tortarolo, M. Buttafava, T. Deguchi, F. Villa, S. Koho, L. Pesce, M. Oneto, S. Pelicci, L. Lanzanó, P. Bianchini, C. J. R. Sheppard, A. Diaspro, A. Tosi, and G. Vicidomini, "A robust and versatile platform for image scanning microscopy enabling super-resolution FLIM," Nat. Methods **16**(2), 175–178 (2019).
13. C. Roider, M. Ritsch-Marte, and A. Jesacher, "High-resolution confocal Raman microscopy using pixel reassignment," Opt. Lett. **41**(16), 3825 (2016).
14. K. Fujita, M. Kobayashi, S. Kawano, M. Yamanaka, and S. Kawata, "High-resolution confocal microscopy by saturated excitation of fluorescence," Phys. Rev. Lett. **99**(22), 228105 (2007).
15. M. Yamanaka, Y. Yonemaru, S. Kawano, K. Uegaki, N. I. Smith, S. Kawata, and K. Fujita, "Saturated excitation microscopy for sub-diffraction-limited imaging of cell clusters," J. Biomed. Opt. **18**(12), 1 (2013).
16. R. Oketani, A. Doi, N. I. Smith, Y. Nawa, S. Kawata, and K. Fujita, "Saturated two-photon excitation fluorescence microscopy with core-ring illumination," Opt. Lett. **42**(3), 571 (2017).

17. Y. Nawa, Y. Yonemaru, A. Kasai, R. Oketani, H. Hashimoto, N. I. Smith, and K. Fujita, "Saturated Excitation microscopy using differential excitation for efficient detection of nonlinear fluorescence signals," APL Photonics **3**(8), 080805 (2018).

18. B. Richards and E. Wolf, "Electromagnetic diffraction in optical systems, II. Structure of the image field in an aplanatic system," Proc. R. Soc. Lond. A **253**(1274), 358–379 (1959).

19. C. Eggeling, A. Volkmer, and C. A. M. Seidel, "Molecular photobleaching kinetics of Rhodamine 6G by one- and two-photon induced confocal fluorescence microscopy," ChemPhysChem **6**(5), 791–804 (2005).

20. C. J. R. Sheppard, M. Castello, G. Tortarolo, G. Vicidomini, and A. Diaspro, "Image formation in image scanning microscopy, including the case of two-photon excitation," J. Opt. Soc. Am. A **34**(8), 1339 (2017).

21. C. J. R. Sheppard, M. Castello, G. Tortarolo, T. Deguchi, S. V. Koho, G. Vicidomini, and A. Diaspro, "Pixel reassignment in image scanning microscopy: a re-evaluation," J. Opt. Soc. Am. A **37**(1), 154 (2020).

22. C. J. R. Sheppard, M. Castello, G. Tortarolo, E. Slenders, T. Deguchi, S. V. Koho, G. Vicidomini, and A. Diaspro, "Image scanning microscopy with multiphoton excitation or Bessel beam illumination," J. Opt. Soc. Am. A **37**(10), 1639 (2020).

23. R. Heintzmann, V. Sarafis, P. Munroe, J. Nailon, Q. S. Hanley, and T. M. Jovin, "Resolution enhancement by subtraction of confocal signals taken at different pinhole sizes," Micron **34**(6-7), 293–300 (2003).

24. M. Yamanaka, Y.-K. Tzeng, S. Kawano, N. I. Smith, S. Kawata, H.-C. Chang, and K. Fujita, "SAX microscopy with fluorescent nanodiamond probes for high-resolution fluorescence imaging," Biomed. Opt. Express **2**(7), 1946 (2011).

25. Y. Zhang, P. D. Nallathamby, G. D. Vigil, A. A. Khan, D. E. Mason, J. D. Boerckel, R. K. Roeder, and S. S. Howard, "Super-resolution fluorescence microscopy by stepwise optical saturation," Biomed. Opt. Express **9**(4), 1613–1629 (2018).

26. G. P. J. Laporte, N. Stasio, C. J. R. Sheppard, and D. Psaltis, "Resolution enhancement in nonlinear scanning microscopy through post-detection digital computation," Optica **1**(6), 455 (2014).

27. M. G. L. Gustafsson, "Nonlinear structured-illumination microscopy: Wide-field fluorescence imaging with theoretically unlimited resolution," Proc. Natl. Acad. Sci. U. S. A. **102**(37), 13081–13086 (2005).

28. J. Huff, "The Airyscan detector from ZEISS: confocal imaging with improved signal-to-noise ratio and super-resolution," Nat. Methods **12**(12), i–ii (2015).

29. A. G. York, S. H. Parekh, D. D. Nogare, R. S. Fischer, K. Temprine, M. Mione, A. B. Chitnis, C. A. Combs, and H. Shroff, "Resolution doubling in live, multicellular organisms via multifocal structured illumination microscopy," Nat. Methods **9**(7), 749–754 (2012).

30. S. Li, J. Wu, H. Li, D. Lin, B. Yu, and J. Qu, "Rapid 3D image scanning microscopy with multi-spot excitation and double-helix point spread function detection," Opt. Express **26**(18), 23585 (2018).